

DynaHull: Density-centric Dynamic Point Filtering in Point Clouds

Pejman Habibiroudkenar^{1*}, Risto Ojala² and Kari Tammi³

^{1,2,3}Mechanical Engineering, Aalto University, , Espoo, 02150, Uusimaa, Finland.

*Corresponding author(s). E-mail(s): pejman.habibiroudkenar@aalto.fi;
Contributing authors: risto.j.ojala@aalto.fi; kari.tammi@aalto.fi;

Abstract

In the field of indoor robotics, accurately navigating and mapping in dynamic environments using point clouds can be a challenging task due to the presence of dynamic points. These dynamic points are often represented by people in indoor environments, but in industrial settings with moving machinery, there can be various types of dynamic points. This study introduces DynaHull, a novel technique designed to enhance indoor mapping accuracy by effectively removing dynamic points from point clouds. DynaHull works by leveraging the observation that, over multiple scans, stationary points have a higher density compared to dynamic ones. Furthermore, DynaHull addresses mapping challenges related to unevenly distributed points by clustering the map into smaller sections. In each section, the density factor of each point is determined by dividing the number of neighbors by the volume these neighboring points occupy using a convex hull method. The algorithm removes the dynamic points using an adaptive threshold based on the point count of each cluster, thus reducing the false positives. The performance of DynaHull was compared to state-of-the-art techniques, such as ERASOR, RemoveIt, OctoMap, and a baseline statistical outlier removal from Open3D, by comparing each method to the ground truth map created during a low activity period in which only a few dynamic points were present. The results indicated that DynaHull outperformed these techniques in various metrics, noticeably in the Earth Mover's Distance. This research contributes to indoor robotics by providing efficient methods for dynamic point removal, essential for accurate mapping and localization in dynamic environments.

Keywords: Dynamic Points Removal, Point Cloud, SLAM, ConvexHull

1 Introduction

Autonomous robotics have become increasingly popular in recent years in research in which indoor positioning and navigation systems have been of particular interest [1]. Mapping stands out as a crucial element in the indoor robotics ecosystem, being essential for several tasks, such as localization, robot control, route-planning, perception, and overall system management. Localization in outdoor settings is often supported by GPS systems, but this traditional method lacks accuracy for indoor environments due to the limitations of the line-of-sight (LoS) path from the satellite [2]. Moreover, indoor mapping primarily relies on RGB cameras [3] and 2D LiDAR [4], with fewer studies exploring the utilization of 3D LiDAR for indoor mapping as 3D LiDAR has been mainly used in outdoor environments [5]. To establish an accurate map, the robot must achieve precise localization; conversely, effective localization is contingent upon a clean, stable map. This interdependence is addressed through the implementation of a technique known as Simultaneous Localization and Mapping (SLAM), a concept that has been set in motion over the past three decades [6].

Mapping in highly dynamic environments, such as in a warehouse teeming with moving people and operational automation robots, presents a unique challenge. The mapping process in such settings is prone to capturing 'dynamic points', also known as ghost or phantom points, which can, for example, compromise the accuracy of a robot's localization in subsequent operations. Removing the dynamic points affected by the ghosting effect, not only significantly enhances localization accuracy and reduces drift [7], but can also enable creation of a clean and accurate map capable of being used for various reconstruction purposes. For instance, it can facilitate the generation of a digital representation of the environment; this reconstructed map would provide valuable insights and can be leveraged in multiple applications. In the context of industrial settings, the reconstructed map can be used to optimize material flow and analyze the efficiency of construction operations.

The proposed dynamic point removal method in this study relies on the distinctive difference in density between the stationary and dynamic points. After several scans, the stationary points are close to each other while the dynamic points are sparse due to their movement. The density is calculated at the point level using our algorithm. To alleviate the undistributed point distribution in mapping processes, the filtering algorithm proposed in this study also clusters the map into smaller sections with different densities.

1.1 Contributions

This study introduces a novel density-based dynamic point removal using a convex hull, DynaHull, for point clouds, that is flexible with maps containing non-uniformly distributed points. Furthermore, this research tailors a dynamic points removal process for point clouds in indoor environments, deviating from the conventional dynamic point elimination methods prevalent in outdoor mapping. Our method performed better than state-art-dynamic-point-removal methods in a highly dynamic indoor environment.

2 Related Work

Dynamic points in point clouds resulting from dynamic objects undermine navigational reliability. In response, researchers have developed several strategic approaches, each one addressing dynamic point issue from a different technological and methodological standpoint. These solutions include ray-tracing methods that consider space occupancy, visibility-based methods focusing on logical geometric consistencies, classical and machine-learning segmentation methods using distinctive features, and advanced data partitioning of dynamic points.

2.1 Voxel Ray Casting Methods

Voxel ray-casting methods, commonly known as 'ray-tracing,' effectively manage the removal of dynamic objects by adjusting the likelihood of space being occupied along the path of the ray as referenced in various studies [8–12]. Areas previously occupied by moving objects become increasingly likely to be considered free as more rays intersect with that space. The early work in this domain, grounded in Dempster-Shafer Theory (DST), also known as the theory of belief, utilizes probability equations to determine the occupation status of a voxel. Xiao et al. [8] enhanced the reliability of spatial representations by fusing occupancy information and integrating data from adjacent rays using the Weighted Dempster-Shafer theory. Building on this, Georgi Postica et al. [9] further refined dynamic points detection by discretizing the occupancy representation based on its distance from the sample scan origin in DST, thus significantly reducing false positives and increasing both speed and accuracy. Schauer et al. [10] improved this approach by traversing a voxel occupancy grid along the lines of sight between the sensor to find differences in volumetric occupancy between the scans, resulting in an increase of the number of scans used for calculations and reducing the required parameter tuning to just one: voxel size. To address the computational cost challenges associated with voxel-based methods, the OctoMap [11] method utilized an efficient oct-tree data structure. Building on this, Kin-Zhang et al. [12] further optimized the approach by minimizing the impact of noise and abnormal points in the OctoMap using the Statistical Outlier Removal (SOR) technique for filtering, and Sample Consensus for performing ground segmentation. Despite their precision and utility, ray-tracing methods face the challenge of incidence angle ambiguity. As the range of measurement extends, the ambiguity in the incidence angle of a point increases, leading to the potential misidentification of adjacent ground points as dynamic objects. This limitation has spurred the development of visibility-based techniques.

2.2 Visibility

Visibility-based methods [13–15] operate under the assumption that if a query point is discerned behind a point previously integrated into the map, it indicates that the initial point is dynamic. These approaches require finding an association between a single point and a map point. Consequently, [13, 14] have focused on iteratively updating the dynamic and stationary states by repeatedly fusing multiple measurements and checking the visibility between a query scan and a map. However, pose-estimate errors accumulated in LiDAR motion can render this association inaccurate, thus

raising the possibility of erroneously deleting stationary points. To address this, Kim **Removert** proposed a multiresolution range image-based false prediction-reverting algorithm, also known as Removert. Initially, this method retains certain static points, then progressively reinstates more ambiguous static points by enlarging the query-to-map association window. This approach compensates for errors in LiDAR motion or registration, hence the name "remove, then revert." However, visibility-based methods struggle with occlusion and the elimination of dynamic points at which static points were not detectable behind these dynamic elements commonly known as Irremovable dynamic point, as demonstrated in Fig. 1. This challenge impedes accurately differentiating between static and dynamic points, which is crucial for creating reliable and detailed maps. To address these challenges and reduce false positives, segmentation methods have gained popularity.

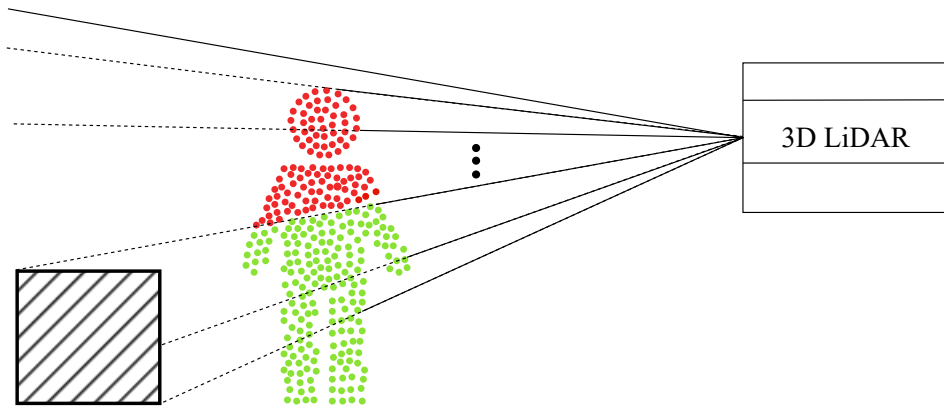


Fig. 1: Irremovable dynamic points are presented in the color red because there are no stationary objects present behind those points. Meanwhile, the green areas are removed because there is a stationary box behind the observed point.

2.3 Segmentation

Segmentation strategies for dynamic point removal in LiDAR data are broadly categorized into classical and machine learning-based methods. Classical approaches, exemplified by Hyungtae Lim et al.'s ERASOR [16], leverage distinctive features of dynamic points. ERASOR, focusing on urban settings, is predicated on the idea that dynamic objects typically touch the ground. This method, by comparing height differences between the original map and the current frame, identifies areas likely containing dynamic elements, and then applies the Region-wise Ground Plane Fitting technique to separate static from dynamic points in these areas.

Machine learning-based methods, as referenced in [17–19, 21, 22], involve segmenting environmental data into distinct entities. This segmentation helps the system

Table 1: Dynamic point removal methods and their limitations

Author	Paper	Method Type	Designed for indoors	Removal time
Xiao et al.	RChange Detection in 3D Point Clouds Acquired by a Mobile Mapping System [8]	Ray tracing	×	Post-mapping
Shishir Pagad et al.	Robust Method for Removing Dynamic Objects from Point Clouds [9]	Ray tracing	×	Post-mapping
Johannes Schauer et al.	The Peopleremover Removing Dynamic Objects From 3-D Point Cloud Data by Traversing a Voxel Occupancy Grid [10]	Ray tracing	×	Post-mapping
Francois Pomerleau et al.	Long-term 3D map maintenance in dynamic environments [13]	Visibility based	×	Post-mapping
R. Ambruş et al.	Meta-rooms: Building and maintaining long term spatial models in a dynamic world [14]	Visibility based	×	Post mapping
Giseop Kim et al.	Remove, then Revert: Static Point cloud Map Construction using Multiresolution Range Images [15]	Visibility based	×	Post-mapping
Hyungtae Lim et al.	ERASOR: Egocentric Ratio of Pseudo Occupancy-based Dynamic Object Removal for Static 3D Point Cloud Map Building [16]	Classical Segmentation	×	Post-mapping
Andres Milioto et al.	RangeNet++: Fast and Accurate LiDAR Semantic Segmentation [17]	Machine learning Segmentation	×	Real-time
Yin Zhou et al.	VoxelNet: End-to-End Learning for Point Cloud Based 3D Object Detection [18]	Machine learning Segmentation	×	Real-time
Xieyuanli Chen et al.	Moving Object Segmentation in 3D LiDAR Data: A Learning-based Approach Exploiting Sequential Data [19]	Machine learning Segmentation	×	Real-time
Xixun Wang et al.	Navigation of Mobile Robots in Dynamic Environments Using a Point Cloud Map [20]	Classical Segmentation	✓	Post-mapping

recognize entities producing ‘ghost tails’. These entities, such as people, cars, and bicycles, are identified and removed from the point cloud. Notably, Ayush Dewan and colleagues [21] devised a method using motion cues for detecting and tracking dynamic objects in urban environments, bypassing the need for prior maps. They employed Bayesian methods for segmentation and RANSAC for motion model estimation. Complementarily, Zhou et al.’s VoxelNet [18] bypassed traditional hand-crafted feature representations, using an end-to-end trainable network for directly processing sparse 3D points. This has significantly improved LiDAR-based detection of cars, pedestrians, and cyclists. Furthermore, [22] introduced PointRCNN, a two-stage framework for 3D object detection from point clouds, which has advanced proposal generation and refinement techniques. Despite these advancements, segmentation-based strategies have limitations. A notable challenge is their struggle with unknown classes [23] and incomplete detection in cases of occlusion. This highlights the ongoing need for developing more robust, versatile, and accurate dynamic point segmentation methods in LiDAR data-processing.

2.4 Research Gap

Ray-tracing techniques, while powerful, require significant computational resources and often struggle with incidence angle ambiguity. Conversely, methods based on visibility face difficulties with irremovable dynamic points. Segmentation approaches also pose their own challenges, particularly in processing unknown classes and segmenting under occlusion. Table 1 provides a comprehensive comparison of the aforementioned methods. Notably, the most dynamic object removal techniques have been applied in outdoor settings, to best of our knowledge, with the exception of [20] which has been used indoors to create a 2D-occupancy map rather than a dynamic-free point cloud. This study focuses on indoor environments characterized by slower movement dynamics compared to outdoor settings. It aims to detect dynamic points without needing pre-trained data and while addressing incidence angle ambiguity in ray tracing and irremovable dynamic point challenges present in visibility-based methods. The proposed approach, DynaHull, which centers on density calculation, is not limited to the challenges explained before as it does not require a prior map and is capable of addressing incidence angle ambiguity and irremovable dynamic point by evaluating each point dynamic feature based on its surrounding points. Furthermore, occlusion also becomes less severe since the density of the point is not related to the viewing angle. By capitalizing on these strengths, the proposed method holds promise for robust and efficient dynamic point removal in indoor environments.

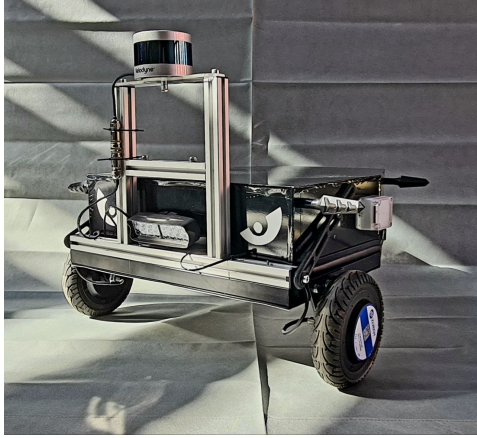
3 Methodology

This section is divided into three parts: "Equipment and Mapping", "DynaHull Algorithm", and "Validation". The first part offers details about the testing robot and the testing environment. The subsequent sub-section explains the DynaHull algorithm and its advantages. Lastly, "Validation" compares our method to other state-of-the-art methods.

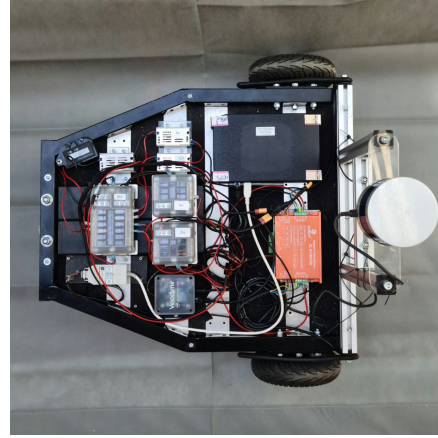
3.1 Equipment and Mapping

The map containing dynamic points was collected using a differential wheel robot named DBot. DBot is equipped with tools, notably the Velodyne VLP 16 sensor, which captures 3D spatial points. The sensor has a 100-meter range and a 30-degree field of view. For optimal coverage, the sensor is mounted at the top of the DBot, as illustrated in Fig 2. The mapping in this study is accomplished by using an HDL graph slam package provided by Koide [24] in ROS (Robotic Operating System) .

In this study, the map was created in the form of point cloud data (PCD) in an indoor environment at a university covering an area of approximately 150 square meters during a demo event in which about 100 people and numerous dynamic objects were present in the robots proximity. The maximum range of the Velodyne VLP16 was set to 75 meters and default parameters were used for HDL graph slam parameters.



(a) Dbot from side



(b) Dbot from top

Fig. 2: Dbot- The robot used for collecting the Data

ConvexHull with Volume of $0.0089 m^3$ ConvexHull with Volume of $0.0599 m^3$

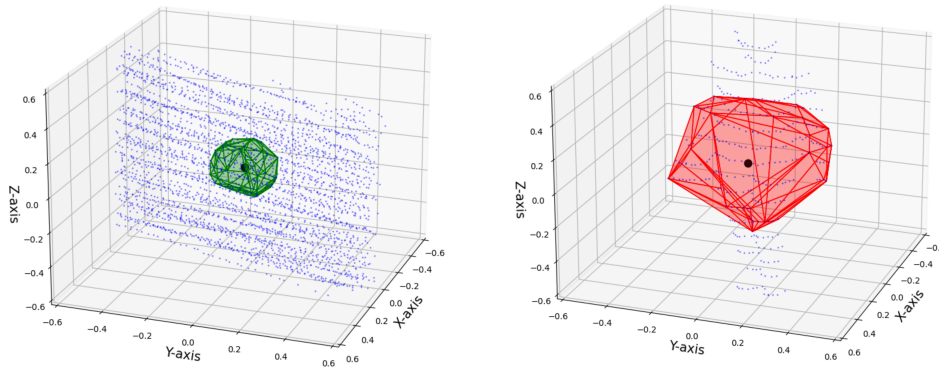


Fig. 3: Estimating convex hull volume between stationary and dynamic points: The left figure represents the stationary area (wall), while the picture on the right illustrates the dynamic area (human).

3.2 DynaHull

The DynaHull method capitalizes on the observation that, after several scans, stationary points have a smaller convex hull volume compared to dynamic ones, as demonstrated in Fig 3.

On completing the mapping, the DynaHull process removes dynamic points as follows (the flowchart is illustrated in Fig. 4): (1) DynaHull segments the ground points by

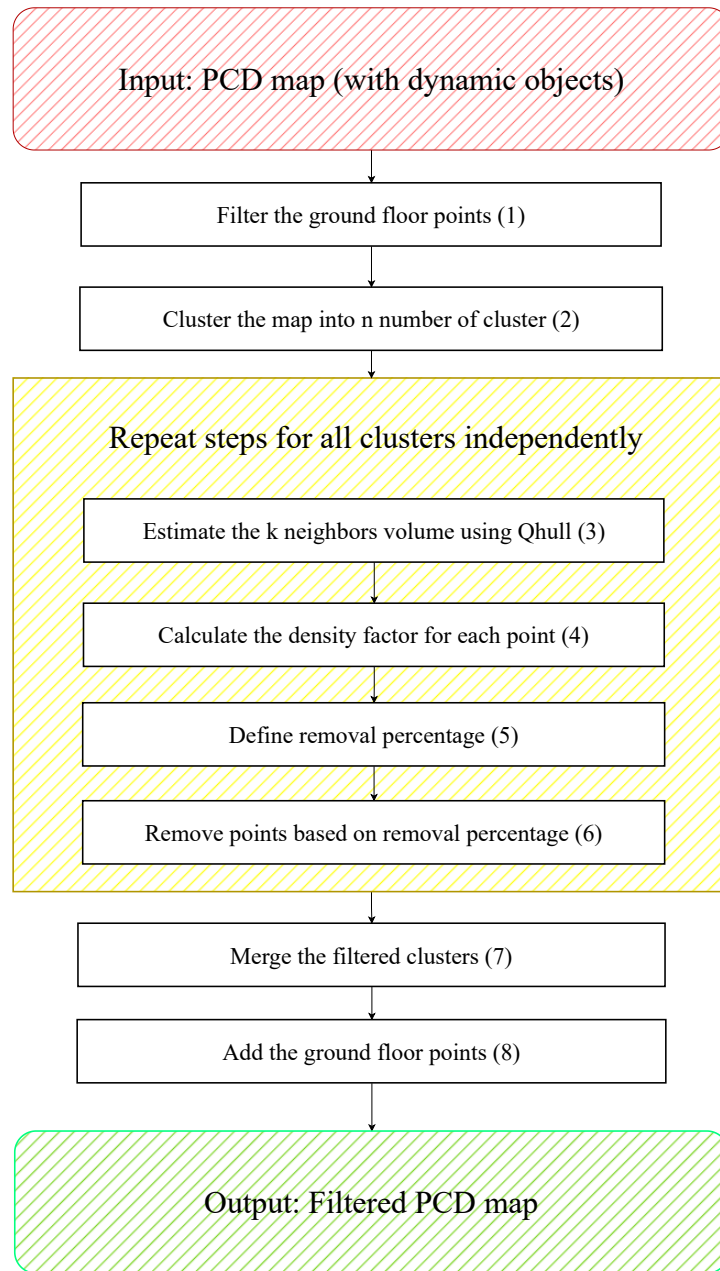


Fig. 4: Flowchart of DynaHull method

estimating the slope of the ground points plane inspired by [25] and segments the floor points accordingly. (2) The map, free from ground points, is divided into N_c (clusters) clusters using Kmeans from [26]. This division helps to manage points that are non-uniformly distributed during mapping. (3) After clustering, nearest neighbor distances (in this study, $k = 75$ number of nearest neighbors) of each point are calculated using sklearn’s efficient KDtree [26]. These distances are then used to calculate the convex hull, which is the smallest convex set containing a given set of points. DynaHull integrates a divide-and-conquer algorithm known as Quickhull from Scipy [27] to efficiently calculate the convex hull volumes (described in detail in the next paragraph). (4) After calculating the convex hull for each point, the point density factor is determined by dividing k neighbor counts by the volume of each convex hull point. (5) After assigning a density factor for each point, a removal percentage is defined, ranging from 5 to 20 percent depending on the point count of the cluster. In other words, the clusters with low point counts will have a lower removal percentage, while the removal percentage increases as the cluster point count increases. This allows the algorithm to be flexible for areas with sparse stationary points which may be due to LiDAR expansion problems or mapping limitations, such as obstacles or inaccessibility. (6) By incrementally increasing a threshold value based on the variances of the previously calculated density factors from zero, points with low density factors are removed until the required removal percentage in each cluster is achieved. These tasks are achieved by utilizing Open3D [28] and numpy [29]. (7) This process is repeated for all clusters, and on completing the last cluster, these refined clusters are merged to reconstruct the map. (8) Finally, the ground floors are added back to the point cloud completing the DynaHull algorithm.

The Quick hull in Step (4) operates as follows:

- Initialization: The algorithm begins by identifying the extreme points on each axis (the smallest and largest) which are key components of the convex hull. Using these points, it forms an initial shape, often a tetrahedron.
- Face Processing: Each face of the initial shape is examined to find the point farthest from it, known as the "furthest point."
- Horizon Edge Search: For each face being examined, the algorithm searches for the "horizon edge" at which a line from the furthest point intersects the shape. Faces visible from the furthest point are marked for removal.
- Constructing New Faces: Marked faces are removed, and new faces are created using the horizon edges as a base, linking the furthest point to these edges.
- Termination: This recursive process continues until no more points are found outside the convex hull. The algorithm concludes when no additional points can be seen from any face of the shape. The volume is returned by summing the volumes of the tetrahedrons. The volume of each tetrahedron is calculated using Equation 1, where \mathbf{A} , \mathbf{B} , \mathbf{C} , and \mathbf{D} represent the four vertices of the tetrahedron.

$$V_{tetrahedrons} = \frac{1}{6} |(\mathbf{A} - \mathbf{D}) \cdot ((\mathbf{B} - \mathbf{D}) \times (\mathbf{C} - \mathbf{D}))| \quad (1)$$

3.3 Validation

Our methodology is evaluated using the DynamicMap Benchmark [12] by Kin-Zhang et al. consisting of well-known algorithms, such as ERASOR [16], Removert [15], and an improved version of OctoMap [11]. Additionally, we incorporate the Statistical Outlier Removal (SOR) from Open3D [28], referred to as O3D. For ERASOR, the configuration for a semi-indoor environment from DynamicMap Benchmark was selected without any modifications. In Removert, the sequence field of the view parameter was adjusted from 50 to 29, aligning with the 30-degree FOV of the Velodyne VLP-16 used in our study. The OctoMap parameters remained unchanged. For statistical outlier removal of O3D, the number of neighbors was set to 100, and the standard deviation ratio was set to 1.

The core evaluation metric compares the map outputs of each method with a reference ground truth map created in a low-activity environment. Any ghost trails made by the robot operator were manually removed using the CloudCompare program. To compare generated maps to the ground truth, the distances of each point in the maps of each method are calculated to its closest point in the ground truth map. Afterwards, the mean absolute error (MAE), variance, root mean square error (RMSE) and 90th percentile error of these distance are recorded. Further comparisons employed the Chamfer Distance [30] and Earth Mover’s Distance (EMD) [31] to assess the similarity between the methods and the ground truth map. The Chamfer Distance is calculated by computing the average of the squared distances from each point in one point cloud to its nearest point in the other point cloud, and vice versa, with a lower value indicating a closer match. EMD, also known as the Wasserstein distance, measures the minimum ‘work’ required to transform one point cloud into another. In our study, the EMD is calculated using the ‘emd2’ function from the Python Optimal Transport (POT) library, with maps uniformly downsampled to reduce computational requirements.

Finally, this paper demonstrates the odometry performance of a map filtered by DynaHull and compares it with the odometry performance of a ground truth map and a dynamic map obtained by scan-matching live LiDAR data to each global map. Odometry data is collected using the ‘HDL localization’ package provided by Koide [24]. The live LiDAR data is replayed using the ROS system for all maps to ensure a fair comparison.

4 Results

For each point in the map, the minimum distance to its corresponding point in the second map (ground truth map) is calculated. The mean and variances of these distances are depicted in Fig. 5. It is evident that DynaHull has the lowest mean and variance. Although the O3D map has the second lowest mean, its variance is higher than that of the Octomap. ERASOR has the highest mean and variances among all the methods.

Table 2 provides a comparison between the filtered map and ground truth in five metrics, namely MAE, RMSE, 90th percentile error, CD, and EMD. Table 2 demonstrates that the similarity of the DynaHull filtered map with ground truth is higher than that of other methods, particularly in the Earth Mover’s Distance.

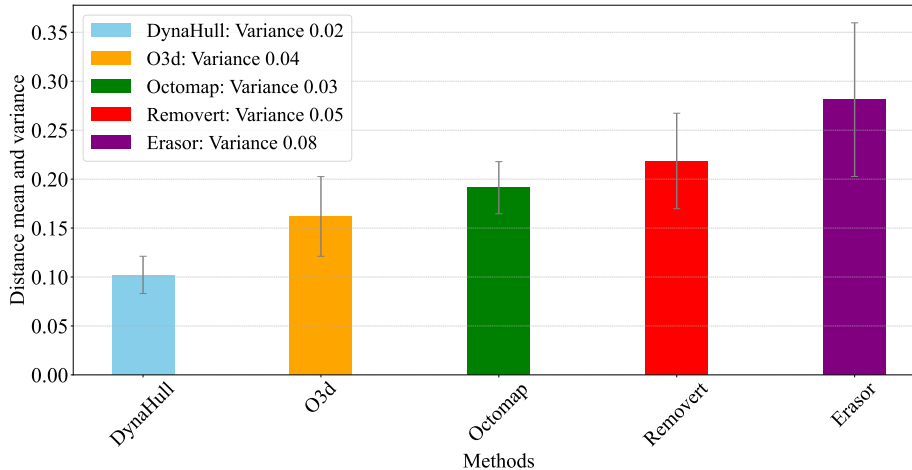


Fig. 5: Mean and variance of distances between the points in each method compared to the ground truth

Table 2: Methods comparison between DynaHull and other methods

File Names	MAE	RMSE	90 Percentile Errors	CD	EMD
DynaHull	0.102	0.312	0.184	4.784	0.766
Removert	0.2185	0.459	0.4085	5.669	2.131
O3D	0.161	0.398	0.311	6.425	2.444
OctoMap	0.191	0.433	0.363	6.0418	2.327
ERASOR	0.281	0.522	0.602	7.375	2.753

To provide a visual comparison between all methods, Fig. 6 shows dynamic and stationary points identified by each method in red and green colors, respectively. Note that for a better visual comparison, the ground and ceiling points in each map have been removed. On examining the figure, it is evident that other methods have excessively removed points from the walls which should be considered stationary. While Removert, O3D, and OctoMap are capable of removing the humans walking in the map, ERASOR struggles to do so.

To emphasize the importance of filtering and the effectiveness of DynaHull in localization, we compared the localization performance of a robot using a dynamic map, a DynaHull-filtered map, and a ground truth map. The corresponding odometry is presented in Fig. 7. The figure illustrates that the DynaHull-filtered map excels in localizing similarly to the ground truth map, while the robot fails to localize itself in a dynamic map. The failure was particularly evident in turns; although the robot

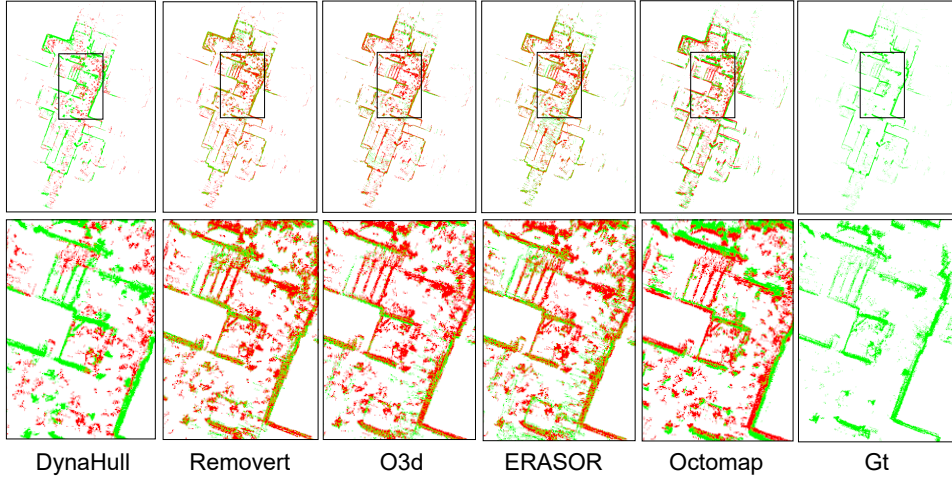


Fig. 6: Comparison between the DynaHull, Removert, O3D, ERASOR, OctoMap, and ground truth. The green points indicate the point at which each method is considered to be stationary whereas the red parts demonstrate the dynamic points.

manages to localize itself during the first two turns in the dynamic map, it completely fails in subsequent turns.

5 Discussion

The primary objective of this study was to improve the accuracy of indoors dynamic points filtering through density filtering. To reach this, a novel density-based method was developed. The proposed algorithm had a few parameters which affect the performance, mainly, the neighboring points count k and removal percentage. In terms of the neighboring points, a larger number might result in denser point clouds with a higher confidence of stationary points. However, an extensive increase of the k value results in more computational power. Another factor influencing the performance of our method is the removal percentage. Increasing the removal percentage value enhances the confidence of dynamic point elimination, but an excessive value may lead to the removal of stationary points.

In comparison with Table 2, the DynaHull method outperformed other techniques in all metrics. In indoor environments, other methods might face challenges in effectively performing when objects show limited dynamism. Furthermore, while other methods utilized 32- or 64-channel LiDARs, our study employed a 16-channel LiDAR. This could explain the reason for these outdoor environment methods underperforming. This distinction is noteworthy as a higher point count is advantageous. This is notably more visible with the ERASOR method as the algorithm was built on the premise of the dynamic points being in contact with the ground. However, since the 16-channel LiDAR does not provide a sufficient number of ground points with

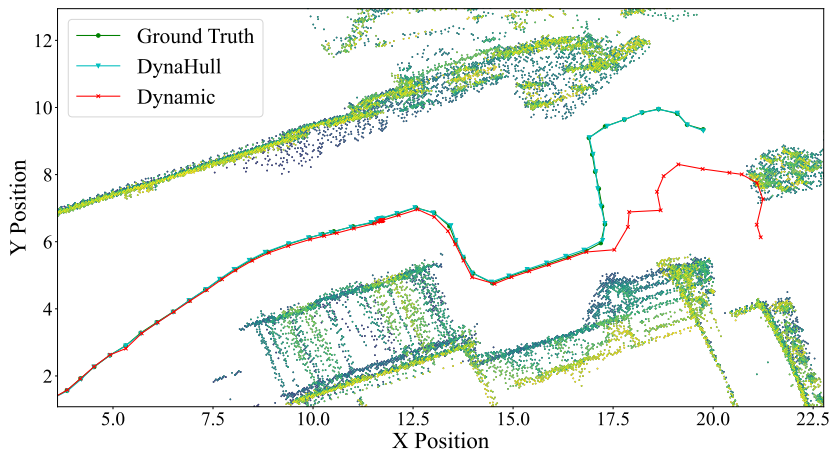


Fig. 7: Odometry comparison between the ground truth, DynaHull, and Dynamic Map: The robot fails to localize itself after the third turn in dynamic map

which the algorithm can detect the dynamic points, ERASOR performs poorly in this scenario. The other contributing factor is the low height of the Velodyne installed on the DBot compared to those installed on top of the autonomous vehicle.

In Figure 6, visually speaking, DynaHull preserved walls better than other methods. In contrast, the other methods falsely removed stationary points, especially in the case of O3D. Although outlier removal methods are efficient in removing dynamic points, they can lead to a noticeable amount of stationary point removal, further emphasizing the importance of specific dynamic point removal techniques such as DynaHull.

One main drawback that affected the filtering performance in all maps was the inaccurate registration of points. Since the mapping was implemented in a highly dynamic environment, the points were not accurately registered due to the presence of a noticeable number of outliers (humans and other dynamic objects). This has caused walls or other stationary features to appear as artificially thickened due to cumulative mapping errors. Improving registration techniques or alignments can enhance the DynaHull method, since thinner walls will decrease the value of the convex hull volume estimates, thereby increasing the density of the stationary points.

6 Summary and Conclusions

This study introduced the DynaHull method for removing dynamic points from point clouds post-mapping. The primary objective was to address the limitations of state-of-the-art techniques, including ray tracing, visibility, and segmentation methods. The results of our study demonstrate the better performance of our methods compared to other state-of-the-art techniques in all the presented metrics, namely, MAE,

RMSE, 90th percentile error, CD, and EMD. The suggested future research directions include applying the DynaHull method across a broader array of scenarios and extending the range of hyperparameter optimization. This approach should incorporate more sophisticated algorithm designs, such as wall detection and machine learning-based segmentation of dynamic objects like humans. Additionally, the development of improved registration techniques tailored for highly dynamic environments is recommended to address the challenges in mapping registration.

References

- [1] A. Loganathan and N. S. Ahmad, “A systematic review on recent advances in autonomous mobile robot navigation,” *Engineering Science and Technology, an International Journal*, vol. 40, p. 101343, 2023.
- [2] T. Kim Geok, K. Zar Aung, M. Sandar Aung, M. Thu Soe, A. Abdaziz, C. Pao Liew, F. Hossain, C. P. Tso, and W. H. Yong, “Review of indoor positioning: Radio wave technology,” *Applied Sciences*, vol. 11, no. 1, 2021.
- [3] A. Macario Barros, M. Michel, Y. Moline, G. Corre, and F. Carrel, “A comprehensive survey of visual slam algorithms,” *Robotics*, vol. 11, no. 1, 2022.
- [4] R. Yagfarov, M. Ivanou, and I. Afanasyev, “Map comparison of lidar-based 2d slam algorithms using precise ground truth,” 11 2018.
- [5] L. Huang, “Review on lidar-based slam techniques,” pp. 163–168, 11 2021.
- [6] J. Leonard and H. Durrant-Whyte, “Simultaneous map building and localization for an autonomous mobile robot,” in *Proceedings IROS '91:IEEE/RSJ International Workshop on Intelligent Robots and Systems '91*, pp. 1442–1447 vol.3, 1991.
- [7] S. Zhao, Z. Fang, H. Li, and S. Scherer, “A robust laser-inertial odometry and mapping method for large-scale highway environments,” pp. 1285–1292, 11 2019.
- [8] W. Xiao, B. Vallet, and N. Paparoditis, “Change detection in 3d point clouds acquired by a mobile mapping system,” *ISPRS Annals of Photogrammetry, Remote Sensing and Spatial Information Sciences*, vol. II-5/W2, pp. 331–336, 10 2013.
- [9] G. Postica, A. Romanoni, and M. Matteucci, “Robust moving objects detection in lidar data exploiting visual cues,” 10 2016.
- [10] J. Schauer and A. Nüchter, “The peopleremover—removing dynamic objects from 3-d point cloud data by traversing a voxel occupancy grid,” *IEEE Robotics and Automation Letters*, vol. 3, no. 3, pp. 1679–1686, 2018.

- [11] A. Hornung, K. Wurm, M. Bennewitz, C. Stachniss, and W. Burgard, “Octomap: An efficient probabilistic 3d mapping framework based on octrees,” *Autonomous Robots*, vol. 34, 04 2013.
- [12] Q. Zhang, D. Duberg, R. Geng, M. Jia, L. Wang, and P. Jensfelt, “A dynamic points removal benchmark in point cloud maps,” *arXiv preprint arXiv:2307.07260*, 2023.
- [13] F. Pomerleau, P. Krüsi, F. Colas, P. Furgale, and R. Siegwart, “Long-term 3d map maintenance in dynamic environments,” in *2014 IEEE International Conference on Robotics and Automation (ICRA)*, pp. 3712–3719, 2014.
- [14] R. Ambrus, N. Bore, J. Folkesson, and P. Jensfelt, “Meta-rooms: Building and maintaining long term spatial models in a dynamic world,” in *2014 IEEE/RSJ International Conference on Intelligent Robots and Systems*, pp. 1854–1861, 2014.
- [15] G. Kim and A. Kim, “Remove, then revert: Static point cloud map construction using multiresolution range images,” in *2020 IEEE/RSJ International Conference on Intelligent Robots and Systems (IROS)*, pp. 10758–10765, 2020.
- [16] H. Lim, S. Hwang, and H. Myung, “Eraser: Egocentric ratio of pseudo occupancy-based dynamic object removal for static 3d point cloud map building,” *IEEE Robotics and Automation Letters*, vol. 6, pp. 2272–2279, 2021.
- [17] A. Milioto, I. Vizzo, J. Behley, and C. Stachniss, “Rangenet ++: Fast and accurate lidar semantic segmentation,” in *2019 IEEE/RSJ International Conference on Intelligent Robots and Systems (IROS)*, pp. 4213–4220, 2019.
- [18] Y. Zhou and O. Tuzel, “Voxelnet: End-to-end learning for point cloud based 3d object detection,” in *2018 IEEE/CVF Conference on Computer Vision and Pattern Recognition (CVPR)*, (Los Alamitos, CA, USA), pp. 4490–4499, IEEE Computer Society, jun 2018.
- [19] X. Chen, S. Li, B. Mersch, L. Wiesmann, J. Gall, J. Behley, and C. Stachniss, “Moving object segmentation in 3d lidar data: A learning-based approach exploiting sequential data,” *IEEE Robotics and Automation Letters*, vol. PP, pp. 1–1, 06 2021.
- [20] X. Wang, Y. Mizukami, M. Tada, and F. Matsuno, “Navigation of a mobile robot in a dynamic environment using a point cloud map,” *Artificial Life and Robotics*, vol. 26, 07 2020.
- [21] A. Dewan, T. Caselitz, G. D. Tipaldi, and W. Burgard, “Motion-based detection and tracking in 3d lidar scans,” in *2016 IEEE International Conference on Robotics and Automation (ICRA)*, pp. 4508–4513, 2016.

- [22] S. Shi, X. Wang, and H. Li, “Pointrcnn: 3d object proposal generation and detection from point cloud,” in *2019 IEEE/CVF Conference on Computer Vision and Pattern Recognition (CVPR)*, pp. 770–779, 2019.
- [23] K. Wong, S. Wang, M. Ren, M. Liang, and R. Urtasun, “Identifying unknown instances for autonomous driving,” *ArXiv*, vol. abs/1910.11296, 2019.
- [24] K. Koide, J. Miura, and E. Menegatti, “A portable three-dimensional lidar-based system for long-term and wide-area people behavior measurement,” *International Journal of Advanced Robotic Systems*, vol. 16, 02 2019.
- [25] M. Himmelsbach, F. v. Hundelshausen, and H.-J. Wuensche, “Fast segmentation of 3d point clouds for ground vehicles,” in *2010 IEEE Intelligent Vehicles Symposium*, pp. 560–565, 2010.
- [26] L. Buitinck, G. Louppe, M. Blondel, F. Pedregosa, A. Mueller, O. Grisel, V. Niculae, P. Prettenhofer, A. Gramfort, J. Grobler, R. Layton, J. VanderPlas, A. Joly, B. Holt, and G. Varoquaux, “API design for machine learning software: experiences from the scikit-learn project,” in *ECML PKDD Workshop: Languages for Data Mining and Machine Learning*, pp. 108–122, 2013.
- [27] P. Virtanen, R. Gommers, T. E. Oliphant, M. Haberland, T. Reddy, D. Cournapeau, E. Burovski, P. Peterson, W. Weckesser, J. Bright, S. J. van der Walt, M. Brett, J. Wilson, K. J. Millman, N. Mayorov, A. R. J. Nelson, E. Jones, R. Kern, E. Larson, C. J. Carey, Í. Polat, Y. Feng, E. W. Moore, J. VanderPlas, D. Laxalde, J. Perktold, R. Cimrman, I. Henriksen, E. A. Quintero, C. R. Harris, A. M. Archibald, A. H. Ribeiro, F. Pedregosa, P. van Mulbregt, and SciPy 1.0 Contributors, “SciPy 1.0: Fundamental Algorithms for Scientific Computing in Python,” *Nature Methods*, vol. 17, pp. 261–272, 2020.
- [28] Q.-Y. Zhou, J. Park, and V. Koltun, “Open3d: A modern library for 3d data processing,” 2018. cite arxiv:1801.09847Comment: <http://www.open3d.org>.
- [29] C. R. Harris, K. J. Millman, S. J. van der Walt, R. Gommers, P. Virtanen, D. Cournapeau, E. Wieser, J. Taylor, S. Berg, N. J. Smith, R. Kern, M. Picus, S. Hoyer, M. H. van Kerkwijk, M. Brett, A. Haldane, J. F. del Río, M. Wiebe, P. Peterson, P. Gérard-Marchant, K. Sheppard, T. Reddy, W. Weckesser, H. Abbasi, C. Gohlke, and T. E. Oliphant, “Array programming with NumPy,” *Nature*, vol. 585, pp. 357–362, Sept. 2020.
- [30] H. Fan, H. Su, and L. Guibas, “A point set generation network for 3d object reconstruction from a single image,” in *2017 IEEE Conference on Computer Vision and Pattern Recognition (CVPR)*, (Los Alamitos, CA, USA), pp. 2463–2471, IEEE Computer Society, jul 2017.
- [31] R. Flamary, N. Courty, A. Gramfort, M. Z. Alaya, A. Boisbunon, S. Chambon, L. Chapel, A. Corenflos, K. Fatras, N. Fournier, L. Gautheron, N. T.

Gayraud, H. Janati, A. Rakotomamonjy, I. Redko, A. Rolet, A. Schutz, V. Seguy, D. J. Sutherland, R. Tavenard, A. Tong, and T. Vayer, “Pot: Python optimal transport,” *Journal of Machine Learning Research*, vol. 22, no. 78, pp. 1–8, 2021.